Dipyridyl Thiosemicarbazone Chelators with Potent and Selective Antitumor Activity Form Iron Complexes with Redox Activity

Des R. Richardson,*,†,§ Philip C. Sharpe,‡ David B. Lovejoy,†,§ Dakshita Senaratne,‡ Danuta S. Kalinowski,†,§ Mohammad Islam,‡ and Paul V. Bernhardt*,‡

Iron Metabolism and Chelation Program, Department of Pathology, University of Sydney, Sydney, New South Wales 2006, Australia, Iron Metabolism and Chelation Program, Children's Cancer Institute Australia for Medical Research, Randwick, Sydney, New South Wales 2031, Australia, and Centre for Metals in Biology, Department of Chemistry, University of Queensland, Brisbane 4072, Australia

Received May 29, 2006

There has been much interest in the development of iron (Fe) chelators for the treatment of cancer. We developed a series of di-2-pyridyl ketone thiosemicarbazone (**H**DpT) ligands which show marked and selective antitumor activity in vitro and in vivo. In this study, we assessed chemical and biological properties of these ligands and their Fe complexes in order to understand their marked activity. This included examination of their solution chemistry, electrochemistry, ability to mediate redox reactions, and antiproliferative activity against tumor cells. The higher antiproliferative efficacy of the **H**DpT series of chelators relative to the related di-2-pyridyl ketone isonicotinoyl hydrazone (**H**PKIH) analogues can be ascribed, in part, to the redox potentials of their Fe complexes which lead to the generation of reactive oxygen species. The most effective **H**DpT ligands as antiproliferative agents possess considerable lipophilicity and were shown to be charge neutral at physiological pH, allowing access to intracellular Fe pools.

Introduction

The development of iron (Fe) chelators for clinical use has traditionally focused on their use for the treatment of Fe-overload disease such as β-thalassemia major.[1−3] More recently, there has been considerable interest in assessing the antitumor activity of a wide variety of ligands.[4−7] The ability of Fe chelators to inhibit tumor growth is probably associated with several factors. First, tumor cells generally proliferate at a faster rate than their normal counterparts and express higher levels of the transferrin receptor 1 (TfR1)[a] that is necessary for Fe uptake from the serum Fe-transport protein, transferrin (Tf).[8] Second, chelators inhibit Fe-requiring enzymes such as ribonucleotide reductase which catalyzes the rate-limiting step of DNA synthesis.[9−11]

Initial studies assessing the effects of novel chelators on tumor growth were stimulated by reports that the Fe chelator, desferrioxamine (DFO; Figure 1), which is used for the treatment of Fe overload, had antitumor activity in vitro in cell culture,[12] in vivo using animal tumor models,[13] and also in clinical trials.[14−16] This finding was of interest since DFO was not designed specifically for the treatment of cancer and possessed numerous disadvantages such as poor membrane permeability which decreased its antiproliferative activity (for reviews, see refs 4, 17, and 18). Hence, the design of more hydrophobic Fe chelators for the treatment of cancer appeared a worthwhile goal.

Over the last 15 years, our laboratories have been involved in assessing the antitumor activity of the pyridoxal isonicotinoyl hydrazone ($\mathbf{H}_2$PIH; Figure 1) class of Fe chelators (for review, see ref 18). These ligands possess high affinity for Fe^{III} and are simple to synthesize via a Schiff base condensation, enabling the preparation of many analogues that have led to the elucidation of important structure−activity relationships.[19,20] Some of these compounds were shown to possess potent antitumor activity, e.g., 2-hydroxy-1-naphthylaldehyde isonicotinoyl hydrazone (chelator 311 or $\mathbf{H}_2$NIH; Figure 1).[20] Examination of these chelators led to the development of several series of ligands showing significantly greater activity. These include the 2-hydroxy-1-naphthylaldehyde thiosemicarbazone ($\mathbf{H}_2$NT) analogues[21] and di-2-pyridyl ketone isonicotinoyl hydrazone (**H**PKIH) chelators (Figure 1).[22]

Considering the activity of the $\mathbf{H}_2$NT and **H**PKIH chelators, more recently we have synthesized the di-2-pyridyl ketone thiosemicarbazone (**H**DpT) series of ligands which are hybrid molecules of the latter two series of compounds (Figure 1).[23] The **H**DpT class of chelators, in particular the ligand, di-2-pyridyl ketone 4,4-dimethyl-3-thiosemicarbazone (**H**Dp44mT; Figure 1), showed the highest antiproliferative activity of all chelators examined so far.[23] These ligands demonstrated selective antitumor activity, having far less effect on the growth of normal cells.[23] In addition, **H**Dp44mT showed marked activity in vivo, reducing the growth of a murine M109 lung cancer by approximately 50% within 5 days of treatment, while having little effect on normal hematological indices.[23] While **H**Dp44mT could effectively induce cellular Fe deprivation, in initial studies the Fe complex was also shown to be redox active within cells.[23] Hence, it was proposed that the antitumor activity of these

* Authors for correspondence. D.R.R. (biology): phone, +61-2-9036-6548; fax, +61-2-9036-6549; e-mail, d.richardson@med.usyd.edu.au. P.V.B. (chemistry): phone, +61-7-3365-4266; fax, +61-7-3365-4299; e-mail, p.bernhardt@uq.edu.au.

† University of Sydney.

§ Children's Cancer Institute Australia for Medical Research.

‡ University of Queensland.

[a] Abbreviations: 3-AP, 3-aminopyridine-2-carboxaldehyde-thiosemicarbazone; DFO, desferrioxamine; DOX, doxorubicin; **H**DpT, di-2-pyridyl ketone thiosemicarbazone; **H**Dp4aT, di-2-pyridyl ketone 4-allyl-3-thiosemicarbazone; **H**Dp4eT, di-2-pyridyl ketone 4-ethyl-3-thiosemicarbazone; **H**Dp4mT, di-2-pyridyl ketone 4-methyl-3-thiosemicarbazone; **H**Dp44mT, di-2-pyridyl ketone 4,4-dimethyl-3-thiosemicarbazone; **H**Dp4pT, di-2-pyridyl ketone 4-phenyl-3-thiosemicarbazone; $\mathbf{H}_2$NIH, 2-hydroxy-1-naphthylaldehyde isonicotinoyl hydrazone; $\mathbf{H}_2$NT, 2-hydroxy-1-naphthylaldehyde thiosemicarbazone; **H**PKIH, di-2-pyridyl ketone isonicotinoyl hydrazone; $\mathbf{H}_2$PIH, pyridoxal isonicotinoyl hydrazone; IBE, iron-binding equivalent; OC, open-circular; ROS, reactive oxygen species; SC, supercoiled; Tf, transferrin; TfR1, transferrin receptor 1.

10.1021/jm0606342 CCC: $33.50
Published on Web 09/29/2006

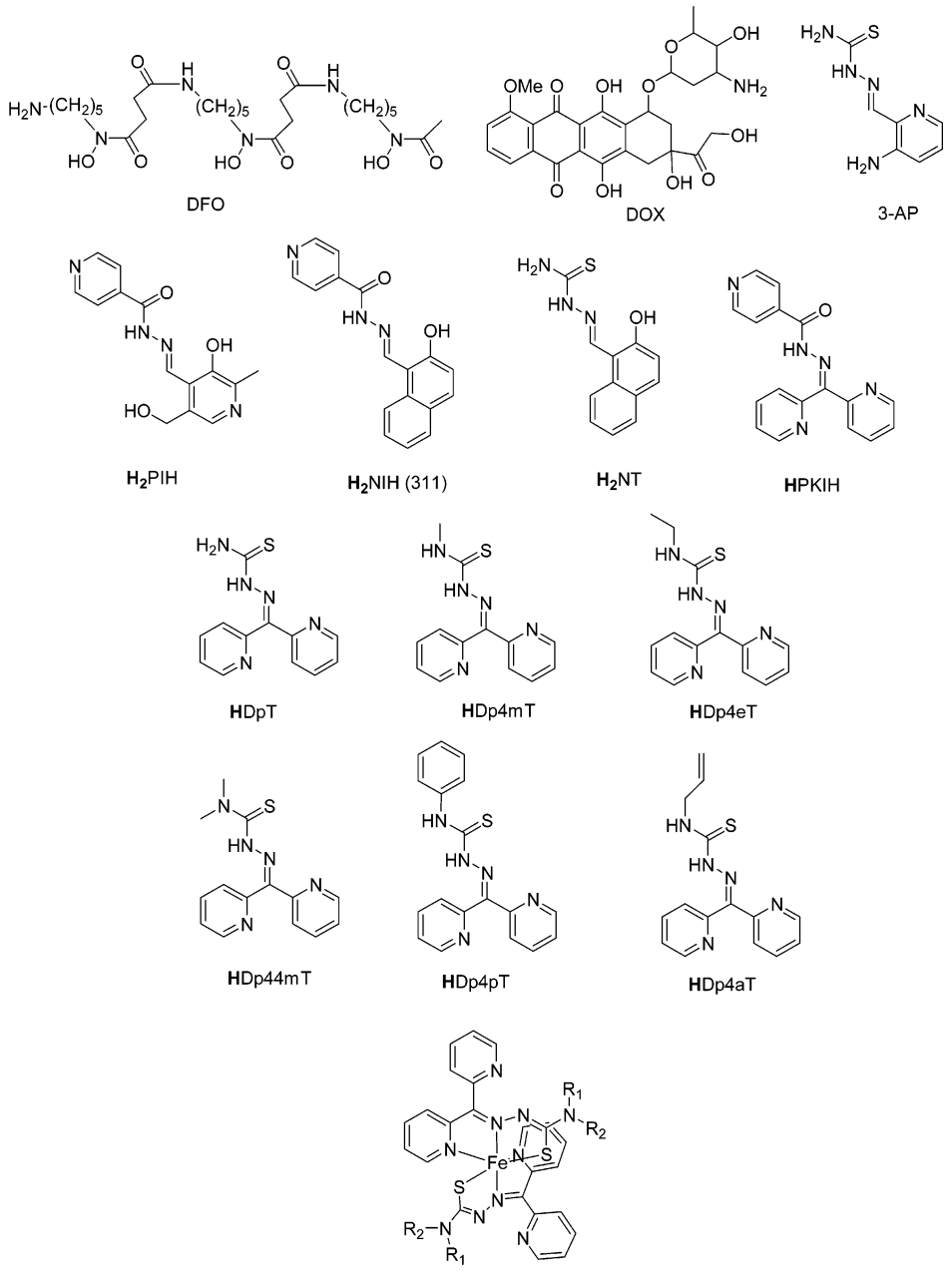

Figure 1. Structural formulae of compounds discussed in this work: desferrioxamine (DFO), doxorubicin (DOX), 3-aminopyridine-2-carboxaldehyde-thiosemicarbazone (3-AP), pyridoxal isonicotinoyl hydrazone (**H**$_2$PIH), 2-hydroxy-1-naphthylaldehyde isonicotinoyl hydrazone (**H**$_2$NIH or 311), 2-hydroxy-1-naphthylaldehyde thiosemicarbazone (**H**$_2$NT), di-2-pyridyl ketone isonicotinoyl hydrazone (**H**PKIH), di-2-pyridyl ketone thiosemicarbazone (**H**DpT), di-2-pyridyl ketone 4-methyl-3-thiosemicarbazone (**H**Dp4mT), di-2-pyridyl ketone 4-ethyl-3-thiosemicarbazone (**H**Dp4eT), di-2-pyridyl ketone 4,4-dimethyl-3-thiosemicarbazone (**H**Dp44mT), di-2-pyridyl ketone 4-phenyl-3-thiosemicarbazone (**H**Dp4pT), di-2-pyridyl ketone 4-allyl-3-thiosemicarbazone (**H**Dp4aT). Schematic representation of a 2:1 Fe complex formed by **H**DpT analogues based on the crystal structures of the closely related **H**PKIH ligands.[39]

compounds relates both to their ability to bind intracellular Fe and form redox-active Fe complexes that generate cytotoxic free radicals.[23]

The current study was designed to comprehensively characterize the biological and chemical properties of Fe complexes of the **H**DpT series of chelators and their redox activity. This work was crucial to understand the antiproliferative activity of this important class of chelators and to determine their structure−activity relationships.

Results and Discussion

X-ray Crystallography of the HDpT Ligands. As representative members of the **H**DpT series, the crystal structures of **H**Dp4mT and **H**Dp4eT have been determined. This was vital in terms of understanding subtle aspects of the protonation of these ligands and, hence, their charge which markedly influences biological activity (see below).[24,25] The crystal structure of **H**Dp4mT in the *C*2/*c* space group has been determined with one independent molecule in the asymmetric unit ($Z = 8$). A view of the ligand is shown in Figure 2A. A feature of the structure is an intramolecular H-bond between the thioamide proton and the adjacent pyridyl group. The bond lengths and angles are typical of other dipyridyl ketone thiosemicarbazones.[26−31] Swearingen and West also reported the crystal structure of **H**Dp4mT in the lower symmetry triclinic space group $P\bar{1}$ with two independent molecules in the asymmetric unit cell ($Z = 4$).[31] Our present analysis is evidently a redetermination of the structure of the same compound but now in the

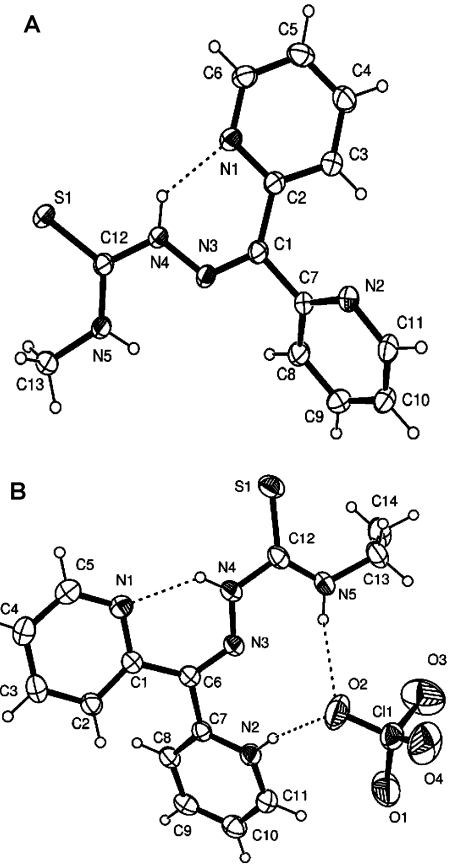

Figure 2. ORTEP view of (A) **H**Dp4mT and (B) [$\mathbf{H}_2$Dp4eT]ClO_4 (30% probability ellipsoids).

Table 1. Crystal Data of the HDpT Ligands, HDp4mT and [H_2Dp4eT]ClO_4

	HDp4mT	[$\mathbf{H}_2$Dp4eT]ClO_4
formula	$C_{13}H_{13}N_5S$	$C_{14}H_{16}ClN_5O_4S$
mol. wt	271.34	385.83
crystal system	monoclinic	monoclinic
a (Å)	19.740(2)	13.967(4)
b (Å)	11.694(1)	8.112(1)
c (Å)	11.514(2)	15.932(2)
α (deg)	90	90
β (deg)	91.391(9)	110.00(1)
γ (deg)	90	90
V (Å^3)	2657.1(6)	1696.2(6)
T (K)	293	293
Z	8	4
space group	*C*2/*c*	$P2_1/n$
μ (Mo Kα, mm^{-1})	0.237	0.379
indep. refs (R_{int})	2329 (0.0491)	2980 (0.0323)
R_1 (obs. data)	0.0382	0.0490
wR_2 (all data)	0.1029	0.1527
CCDC no.	608888	608889

correct space group (Table 1). [The (primitive) reduced cell from our data $a = 11.472$ Å, $b = 11.472$ Å, $c = 11.514$ Å, $\alpha = 88.80°$, $\beta = 88.80°$, $\gamma = 61.28°$, $V = 1329$ Å^3 matches that of Swearingen and West.]

The chelator **H**Dp4eT was crystallized from dilute $HClO_4$ solution to afford X-ray quality crystals of its hydrogen perchlorate salt. As shown in the view of the salt in Figure 2B, the additional proton resides on N2 of a pyridyl ring; specifically the ring not involved in intramolecular H-bonding with the thioamide proton. An interesting bidentate H-bonding interaction between a pair of N−H groups and the perchlorate anion is apparent. Of note is that the Cl1−O2 bond length is significantly longer than the remaining three Cl−O bonds, a consequence of this H-bonding interaction.

Table 2. Protonation Constants and Octanol−Water Partition Coefficients (log *P*) for the HDpT Analogues

ligand	pK_{a1}	pK_{a2}	log *P*
HDpT	9.88 (0.02)	3.91 (0.05)	0.78
HDp4mT	11.14 (0.02)	3.92 (0.04)	3.18
HDp4eT	11.09 (0.02)	3.92 (0.05)	1.23
HDp44mT	9.55 (0.05)	4.29 (0.1)	2.19
HDp4aT	11.01 (0.02)	3.88 (0.04)	1.68
HDp4pT	−	−	1.96

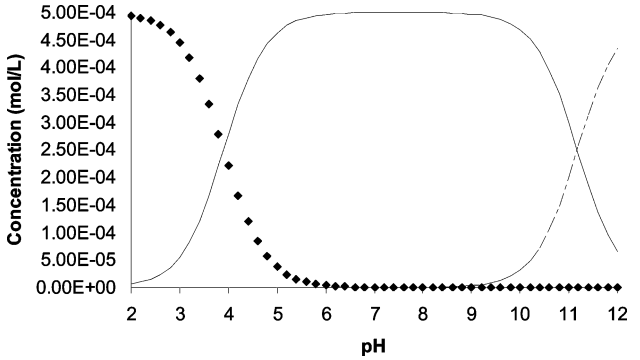

Figure 3. Speciation plot for [$\mathbf{H}_2$Dp4eT]$^+$ (diamonds), **H**Dp4eT (solid curve), and [Dp4eT]$^-$ (broken curve) as a function of pH.

Protonation Constants of the HDpT Ligands. Potentiometric titrations were undertaken to probe the acid−base equilibria associated with each ligand and to determine the pH range over which the chelator is in its charge neutral form. This is important in understanding the passage of the molecule through cell membranes, as charged chelators have poor access.[18,24,25]

The poor aqueous solubility of **H**Dp4pT precluded determination of its protonation constants. The results for the remaining ligands are summarized in Table 2. The higher pK_a corresponds to the $(py)_2C{=}N{-}N\mathbf{H}{-}C{=}S$ group and varies considerably as a function of the substituent on the N-atom at position 4. The lower pK_a is due to protonation of the pyridyl ring seen in Figure 2B. In addition to identifying the site of protonation as N2, the crystal structure of [$\mathbf{H}_2$Dp4eT]ClO_4 explains why N1 is so resistant to protonation, as it is involved in an H-bond with the thioamide group (Figure 2B). The speciation plot for **H**Dp4eT is shown in Figure 3, and it can be seen that the charge neutral form (solid curve) is dominant at physiological pH enabling facile passage across cell membranes. This would explain, at least in part, the high biological activity of these chelators at mobilizing intracellular Fe, preventing Fe uptake from the serum Fe transport protein, transferrin (Tf), and also inhibiting cellular proliferation.[23]

The protonated form (Figure 3, diamonds) becomes dominant below pH 4, while the deprotonated form is only important above pH 11 (Figure 3, broken line). Hence, if these agents are ever given as drugs via the oral route, the low pH of the stomach (pH 1−2) would prevent absorption of the drug at this site as the molecule will be charged.[24] More facile absorption would occur in the small intestine where the higher pH (pH 5−7) would result in a neutral ligand and greater uptake.[24]

Lipophilicity of the HDpT Ligands. The lipophilicity of a chelator has been shown to be an important property with regard to its ability to permeate biological membranes[32] and can be conveniently estimated by its partition coefficient.[33−37] The octanol:water partition coefficients for the chelators were measured (log *P*), and the results appear in Table 2.

Table 3. IC_{50} (μM) Values of 3-Aminopyridine-2-carboxaldehyde-thiosemicarbazone (3-AP), Desferrioxamine (DFO), and the HDpT Series Chelators and their Ferrous and/or Ferric Complexes at Inhibiting the Growth of SK-N-MC Cells after 96 h[a]

chelator/complex	IC_{50} (μM)	*p* value
DFO	8.58 ± 1.65	
Fe^{III}DFO[b]	>25	
3-AP	0.39 ± 0.03	
Fe^{II}3-AP[b]	0.74 ± 0.29	$p > 0.05$ (NS)
Fe^{III}3-AP[b]	0.40 ± 0.03	$p > 0.05$ (NS)
HDpT	5.20 ± 0.44	
$Fe^{II}(DpT)_2$	>6.25	
$[Fe^{III}(DpT)_2]ClO_4$	>6.25	
HDp4mT	0.18 ± 0.02	
$Fe^{II}(Dp4mT)_2$	1.53 ± 0.21	$p < 0.001$
$[Fe^{III}(Dp4mT)_2]ClO_4$	1.02 ± 0.28	$p < 0.001$
HDp4eT	0.05 ± 0.03	
$Fe^{II}(Dp4eT)_2$	1.21 ± 0.47	$p < 0.001$
$[Fe^{III}(Dp4eT)_2]ClO_4$	0.46 ± 0.16	$p < 0.001$
HDp44mT	0.01 ± 0.01	
$Fe^{II}(Dp44mT)_2$	0.42 ± 0.08	$p < 0.001$
$[Fe^{III}(Dp44mT)_2]ClO_4$	0.35 ± 0.02	$p < 0.001$
HDp4aT	0.02 ± 0.01	
$Fe^{II}(Dp4aT)_2$	0.69 ± 0.24	$p < 0.001$
$[Fe^{III}(Dp4aT)_2]ClO_4$	0.68 ± 0.15	$p < 0.001$
HDp4pT	0.01 ± 0.01	
$Fe^{II}(Dp4pT)_2$	0.21 ± 0.05	$p < 0.001$
$[Fe^{III}(Dp4pT)_2]ClO_4$	0.15 ± 0.09	$p < 0.001$

[a] Proliferation was determined by the MTT assay (see Experimental Section for further details). Results are mean ± SD (three experiments). The *p* values were determined using Student's *t*-test and compare the activity of the ligand to its relevant complex. A value of $p > 0.05$ was considered as not significant (NS). [b] Indicates complexes that were made in situ.

It is apparent that the most hydrophilic chelator is **H**DpT, which bears two protons on N4, while all other chelators are more lipophilic due to the presence of one or two hydrophobic substituents (Figure 1). Considering this, it is important to note that **H**DpT shows much lower antiproliferative activity ($IC_{50} = 5.20$ μM; Table 3) at inhibiting the growth of tumor cells than the other **H**DpT chelators ($IC_{50} = 0.01-0.18$ μM; Table 3). Furthermore, **H**DpT was not effective at mobilizing intracellular Fe or preventing Fe uptake from transferrin in contrast to the other analogues which showed similar and marked activity.[23] Hence, the relative hydrophilicity of **H**DpT may lead to lower biological activity relative to the other analogues.

Apart from **H**DpT, log *P* of the remaining five **H**DpT analogues varied from 1.23 to 3.18 (Table 2). For four of the five **H**DpT analogues, log *P* was greater than 1.5, indicating these compounds were moderately lipophilic. In studies examining the $\mathbf{H}_2$PIH class of chelators, optimal activity in releasing ^{59}Fe from reticulocytes was observed when log *P* [free ligand] ≈ 2.8.[38] In addition, high Fe chelation efficacy of a series of diaroylhydrazine Fe chelators was observed when log *P* was 1.7 or greater.[39] Analysis of the biological activity of the five **H**DpT analogues (namely **H**Dp4mT, **H**Dp4eT, **H**Dp44mT, **H**Dp4aT, and **H**Dp4pT) relative to their log *P* value demonstrated no strong statistical correlation (data not shown). In these analyses, the biological activities assessed included the antiproliferative activity of the ligands (Table 3) and also their ability to mobilize Fe from cells and prevent Fe uptake from Tf, which we reported previously.[23]

Characterization of the HDpT−Fe Complexes: Electronic Spectra and Electrochemistry. The Fe coordination chemistry of the **H**DpT analogues remains essentially unexplored, and the biological Fe coordination chemistry of these chelators has not been examined in any detail. Of most relevance to this study was the isolation and characterization of both the Fe^{II} and Fe^{III} complexes of the **H**DpT analogues. The syntheses of all Fe^{II} complexes were conducted under an inert atmosphere as aerobic oxidation to the Fe^{III} analogues was found to be significant in some cases. Once isolated as solids, the ferrous complexes were stable indefinitely. The Fe^{III} complexes were synthesized in a similar fashion except ferric perchlorate was used.

The electronic spectra of the Fe complexes are very sensitive to oxidation state, but less dependent on the substituents present. Table 4 summarizes the spectral data. In addition to intense intraligand electronic transitions in the near UV, the Fe^{II} complexes all exhibit an intense asymmetric band in the range 630−660 nm, which gives them their distinctive green color. This visible transition is of metal-to-ligand ($Fe^{II} \rightarrow$ pyridine) charge-transfer origin and is related to the $Fe^{III/II}$ redox potential (see below). The Fe^{III} complexes exhibit electronic spectra that are somewhat similar to those of the free ligands, although the intraligand bands are shifted into the visible region giving the complexes their dark brown appearance.

Cyclic voltammetry of the Fe complexes was performed in a mixture of MeCN and water (70:30) due to the limited solubility of the complexes in water alone. Totally reversible $Fe^{III/II}$ redox couples were identified in all cases, with $E°$ values varying from +153 to +225 mV vs NHE (Table 4). The peak currents increased linearly with the square root of sweep rate, and the anodic/cathodic current ratio was unity at all sweep rates. As an example, cyclic voltammograms of $[Fe(Dp44mT)_2]ClO_4$ at various sweep rates are shown in Figure 4. The peak potentials and the ratios of the anodic and cathodic current maxima are essentially invariant within the range of sweep rates 20−500 mVs^{-1}, and this is typical behavior for all complexes. That is, the heterogeneous electron-transfer rate is rapid, and both components of the redox are stable. This is consistent with our ability to isolate and characterize both the ferrous and ferric complexes as solids.

The redox potentials of the **H**DpT Fe complexes are 300 to 400 mV lower than those found for the Fe complexes of the structurally related **H**PKIH analogues (ca. +500 mV),[40] and they lie within a range accessible to intracellular oxidants (dioxygen) and reductants such as NADPH, thiols, etc. Indeed, previous studies examining the **H**PKIH analogues and also **H**Dp44mT have demonstrated that these chelators are capable of generating reactive oxygen species (ROS) intracellularly.[23,40,41] Considering the lower redox potentials of the **H**DpT chelators, the facilitation of redox activity should occur more readily than that observed with the **H**PKIH class. Hence, the higher antiproliferative activity of the **H**DpT series of chelators[23] relative to the **H**PKIH class[22] can be ascribed, at least in part, to the electrochemical potentials of their Fe complexes which lead to greater ROS generation. However, this is not the only factor which is important. As described above, the most active **H**DpT ligands possess considerable lipophilicity (Table 2), allowing them to permeate cell membranes and bind Fe pools in tumor cells more readily than less lipid-soluble chelators, e.g., DFO. Hence, the ability of these ligands to bind intracellular Fe and generate ROS is similar to the mechanism of action of the cytotoxic agent, doxorubicin (DOX; Figure 1).[42] The resulting oxidative damage potentiates the antiproliferative activity of the **H**PKIH and **H**DpT chelators compared to $\mathbf{H}_2$NIH or DFO that bind Fe but do not actively redox cycle.[43] We have termed this effect the "double-punch", and it is an important structure−activity relationship that should be encompassed into the design of future ligands for the treatment of cancer.

Table 4. Electronic Spectral Data (MeOH; λ_{max}, nm; ϵ, M^{-1} cm^{-1}) and Electrochemical Data (70:30 MeCN:H_2O) for all **H**DpT Analogue Fe Complexes

L	$Fe^{II}L_2$	$[Fe^{III}L_2]^+$	E^0 (mV vs NHE)
HDpT	644 (ϵ 5 270)	460 (ϵ 6 770)	+165
	365 (ϵ 14 860)	365 (ϵ 12 340)	
HDp4mT	643 (ϵ 8 040)	475 (ϵ 6 950)	+153
	380 (ϵ 22 850)	379 (ϵ 19 240)	
HDp4eT	644 (ϵ 7 450)	463 (ϵ 5 170)	+173
	379 (ϵ 28 830)	380 (ϵ 13 780)	
HDp44mT	646 (ϵ 10 840)	486 (ϵ 10 340)	+166
	390 (ϵ 30 040)	395 (ϵ 32 600)	
HDp4aT	626 (ϵ 3 850)	462 (ϵ 4 320)	+170
	379 (ϵ 26 300)	381 (ϵ 21 700)	
HDp4pT	630 (ϵ 7 200)	469 (ϵ 5 410)	+225
	393 (ϵ 24 540)	368 (ϵ 10 870)	

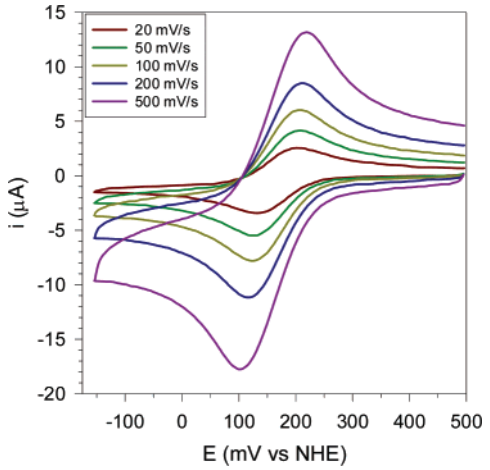

Figure 4. Cyclic voltammograms of $[Fe(Dp44mT)_2]ClO_4$ as a function of sweep rate (mV s^{-1}): 20 (red), 50 (green), 100 (yellow), 200 (blue), and 500 (pink).

Unlike the facile voltammetry seen here for the Fe complexes of the **H**DpT analogues, the electrochemistry of the closely related PKIH−Fe^{II} complexes was complicated by rapid nucleophilic attack by water on the C═N−Fe group upon oxidation to the ferric state.[40] Interestingly and counterintuitively, this may be explained by the exchange of an O-donor atom in the **H**PKIH chelators with an S-donor in the **H**DpT analogues (see Figure 1), stabilizing the higher oxidation state. Clearly, the thiolate S-donor is another structural feature that is relevant for the future design of chelators as antitumor agents.

Effects of the Iron Complexes of HDpT on Cellular Proliferation. Previous studies have demonstrated that complexation of chelators with metals can result in marked alterations in their biological activity.[19,44−46] To assess the effect of complexation with Fe^{II} or Fe^{III} on the antiproliferative activity of the **H**DpT chelators, their Fe complexes were prepared. Two relevant positive controls were also screened, namely DFO which is used for treatment of Fe-overload and the clinically trialed chelator, 3-aminopyridine-2-carboxaldehyde-thiosemicarbazone (3-AP; Figure 1), that was designed for cancer therapy.[10,47] DFO showed relatively low antiproliferative activity (IC_{50}: 8.58 μM), while 3-AP was far more effective (IC_{50}: 0.39 μM; Table 3). As shown in our previous studies, complexation of DFO with Fe^{III} totally prevented its antiproliferative activity, while it had no significant effect on the activity of 3-AP.[10]

Of the **H**DpT analogues, **H**DpT showed the least activity (IC_{50}: 5.20 μM), while **H**Dp44mT, **H**Dp4pT, **H**Dp4aT, and **H**Dp4eT showed similar and marked efficacy at inhibiting proliferation (IC_{50}: 0.01−0.05 μM; Table 3). **H**Dp4mT was less active than these latter four analogues, but far more effective than **H**DpT (Table 3).

All of the Fe^{II} and Fe^{III} complexes of the **H**DpT analogues, except the relatively benign **H**DpT, resulted in significantly ($p < 0.001$) decreased antiproliferative activity compared to their free ligands (Table 3). In fact, complexation with Fe resulted in the IC_{50} increasing by a factor of 6−42 times. Examining the same ligand, there were no significant differences between the IC_{50} values of its Fe^{II} or Fe^{III} complexes, suggesting that each oxidation state resulted in similar effects. In fact, it is possible that these oxidation states exist in equilibrium within the cell, and the electrochemistry of the Fe complexes would suggest facile interconversion between the redox states, as described above. The decreased antiproliferative activity of the Fe complexes, relative to their respective ligands, could be explained by (1) the complex having less intracellular access preventing it from damaging the cell, and/or (2) the preformed complex blocking the chelation of Fe from sensitive cellular pools involved in proliferation, e.g., ribonucleotide reductase. The current results with the Fe complexes of the **H**DpT analogues contrast with results obtained with the Fe complexes of two closely related **H**PKIH analogues.[48] In fact, it was shown that the Fe complexes of these latter chelators resulted in a 3−6-fold increase in activity relative to their ligands.[48] Hence, while precomplexation of the **H**PKIH complexes with Fe may be beneficial for the administration of these compounds to enhance their activity, this would not be advantageous for the **H**DpT analogues.

Plots comparing the measured redox potentials versus the antiproliferative activity of the ligands and their Fe^{II} and Fe^{III} complexes were examined to determine if a relationship between these factors existed (data not shown). In this analysis, **H**DpT was excluded as an IC_{50} value was not determined for its Fe^{II} and Fe^{III} complexes. A weak linear relationship was observed between the redox potentials and the antiproliferative activity of the free ligands ($R = -0.55$) and their Fe^{II} ($R = -0.70$) and Fe^{III} complexes ($R = -0.78$). However, while the redox potential and hence the free radical generating activity of these agents plays a role in their antitumor efficacy, it is not the sole factor involved. Thus, a weak linear relationship was observed. As discussed previously, the ability of the ligand to enter the cell, determined by both the log *P* and charge at physiological pH, are other significant aspects which determine antitumor activity.

Effects of the Iron Complexes of HDpT Analogues on Ascorbate Oxidation. Our electrochemistry studies reported above clearly indicate that the redox potentials of the Fe complexes of the **H**DpT analogues are suitable to allow facile redox cycling. However, the ability of **H**Dp44mT to directly catalyze oxidation of a physiological substrate has not been shown. Considering this, the effect of the **H**DpT chelators on the oxidation of ascorbate was determined (Figure 5A). The

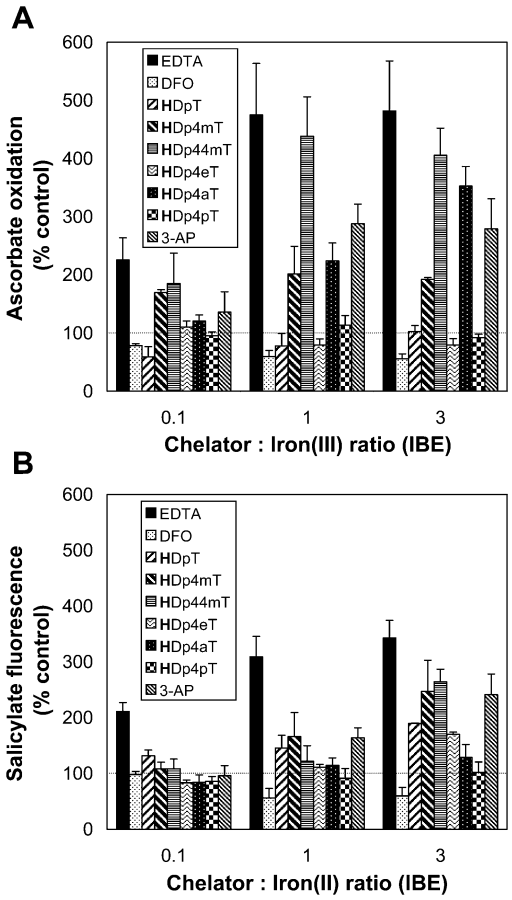

Figure 5. Effect of various Fe chelators on (A) the degree of ascorbate oxidation and (B) the hydroxylation of benzoate in the presence of Fe^{II} and hydrogen peroxide. (A) Ascorbate oxidation studies: chelators at iron-binding equivalent (IBE) ratios of 0.1, 1, and 3 were incubated in the presence of Fe^{III} (10 μM) and ascorbate (100 μM). The UV−vis absorbance at 265 nm was recorded after 10 and 40 min, and the difference between the time points was calculated. (B) Benzoate hydroxylation studies: chelators at IBE ratios of 0.1, 1, and 3 were incubated for 1 h at room temperature in the presence of Fe^{II} (30 μM), hydrogen peroxide (5 mM), and benzoate (1 mM). The fluorescence of hydroxylated benzoate was measured at 308 nm excitation and 410 nm emission. Results are mean ± SEM (three experiments).

chelators EDTA and DFO were used as positive and negative controls, respectively, as their activity has been well characterized.[40,49,50]

In this assay, EDTA increased ascorbate oxidation to 475% and 482% of the control at an iron-binding equivalent (IBE; see Experimental Section) of 1 and 3, but had less effect at an IBE of 0.1, as shown in previous studies (Figure 5A).[10,41,50] DFO inhibited the reaction to 79, 60, and 59% of the control at IBEs of 0.1, 1, and 3, respectively (Figure 5A). These results can be explained by the fact that the $Fe^{III/II}$ redox potential of the fully formed EDTA complex in water at pH 7 is ca. +90 mV vs NHE (depending on the supporting electrolyte),[51] allowing facile redox cycling and ascorbate oxidation. On the other hand, DFO readily binds Fe^{III}, but the low $Fe^{III/II}$ redox potential (−486 mV vs NHE) of this complex[52] leads to negligible rates of ascorbate oxidation.[50]

To provide direct comparison with the **H**DpT chelators and as a further positive control, we also examined the thiosemicarbazone chelator, 3-AP.[53−56] In agreement with our previous studies,[10] 3-AP was active at increasing ascorbate oxidation at all IBEs, but particularly at an IBE of 1 and 3 (Figure 5A). However, the **H**DpT chelators varied in their ability to promote the Fe^{III}-mediated oxidation of ascorbate. **H**Dp4mT, **H**Dp4aT, and **H**Dp44mT increased ascorbate oxidation at all IBEs, but were most effective at an IBE of 1 and 3 (Figure 5A). Chelator **H**Dp44mT showed the greatest activity, being comparable to EDTA, and increased the oxidation of ascorbate to 439% and 406% of the control at IBEs of 1 and 3, respectively. At the extremes, the Fe−DpT analogue complexes with the lower $Fe^{III/II}$ redox potentials (e.g., **H**Dp44mT, Table 3) resulted in greater ascorbate oxidation activity than those at the higher end (e.g., **H**Dp4pT) although there were exceptions within this series. If redox potentials are indeed an important component of ascorbate oxidation catalysis, then the greater activity of the lower potential complexes suggests that the rate-limiting step is reoxidation of the ferrous complex by oxygen (the oxidative half reaction) in order for the catalytic cycle to continue. That is, the lower potential ferrous complexes are oxidized more rapidly. However, substituent effects could also be relevant, i.e., steric effects from the N4 alkyl, allyl, and aromatic substituents may affect the way in which the complex interacts with ascorbate.

The results showing the high activity of **H**Dp44mT to catalyze the oxidation of ascorbate are in good agreement with its redox potentials and also our studies in cells examining the oxidation of the fluorescent probe, H_2-DCF-DA.[23] The ascorbate oxidation results suggest that the ferric complexes of **H**Dp44mT, **H**Dp4mT, **H**Dp4aT effectively act as oxidation catalysts. This is in contrast to our results with the closely related **H**PKIH analogues which do not effectively oxidize ascorbate.[40,41] The reasons for the difference between the **H**PKIH analogues and these three **H**DpT chelators is probably explained by their electrochemistry. For the **H**PKIH analogues, the electrochemistry of the PKIH−Fe^{II} complexes was complicated by rapid nucleophilic attack by water on the C=N−Fe group upon oxidation to the ferric state.[40] In other words, the potentially high oxidizing power of the ferric **H**PKIH complexes is lost through nucleophilic attack by hydroxide on the Fe^{III} form.[40] In contrast, the Fe complexes of the **H**DpT analogues enjoy facile interconversion between the Fe^{II} and Fe^{III} states uncomplicated by following chemical reactions (Figure 4). Thus, the ferric complex retains its oxidizing power.

Effects of the Iron Complexes of HDpT Analogues on Benzoate Hydroxylation. The effect of the chelators on Fe^{II}-mediated hydroxyl radical production was measured by monitoring the hydroxylation of benzoate to the fluorescent product salicylate in the presence of Fe^{II} and H_2O_2 (Figure 5B). Again, EDTA and DFO acted as positive and negative controls, respectively.[40,49,50] EDTA stimulated benzoate hydroxylation to 309% and 343% of the control at IBEs of 1 and 3, respectively. In contrast, DFO inhibited the reaction to 56−60% of the control at IBEs of 1 and 3 (Figure 5B). These results were in good agreement with our previous studies.[10,50] The EDTA complex has a sufficiently high $Fe^{III/II}$ potential such that the catalytically active divalent oxidation state is accessible, whereas the divalent Fe−DFO complex is not stable in aerobic solution and cannot catalyze Fenton chemistry.

As shown previously,[10] 3-AP was also active in this assay, markedly increasing benzoate hydroxylation to 164% and 241% of the control at IBEs of 1 and 3, respectively (Figure 5B). The chelators **H**DpT, **H**Dp4eT, **H**Dp4mT, and **H**Dp44mT all increased benzoate hydroxylation, particularly at an IBE of 3 (Figure 5B). In contrast, **H**Dp4aT and **H**Dp4pT had little effect on benzoate hydroxylation compared to the control.

There are several factors that dictate the ability of a chelator to alter the rate of hydroxyl radical generation and benzoate hydroxylation.[40] A ligand can inhibit benzoate hydroxylation

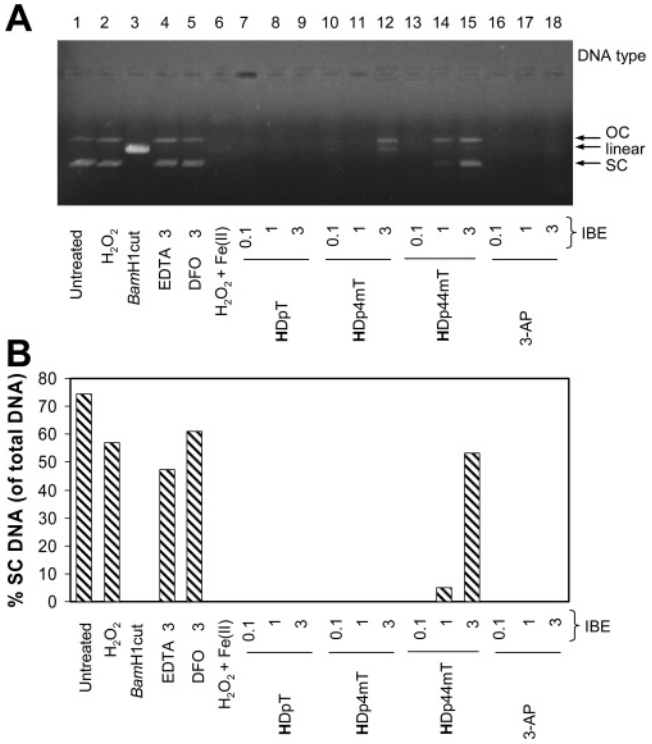

Figure 6. (A) The effect of various Fe chelators on Fenton-mediated plasmid degradation. Chelators at iron-binding equivalent (IBE) ratios of 0.1, 1, and 3 were incubated for 30 min in the presence of Fe^{II} (10 μM), hydrogen peroxide (1 mM), and plasmid DNA (10 μg/mL). (B) Densitometric analysis of the data in panel A, showing the percentage of DNA in its supercoiled (SC) form. The result illustrated is typical of three experiments performed.

by binding Fe^{II} strongly, as is observed with the 2-pyridylcarboxaldehyde isonicotinoyl hydrazone series of chelators[50] or by acting as a radical scavenger. Stimulation of benzoate hydroxylation, as observed with EDTA, **H**DpT, **H**Dp4eT, **H**Dp4mT, and **H**Dp44mT, indicates that these Fe complexes redox cycle rapidly between the ferrous and ferric states. These results are in marked contrast to that observed with the related **H**PKIH chelators that do not stimulate benzoate hydroxylation, which is probably due to the relative stability of the PKIH−Fe^{II} complex.[40] Interestingly, despite their structural and electrochemical similarities to the other **H**DpT analogues, neither **H**Dp4aT nor **H**Dp4pT had any marked effect on benzoate hydroxylation.

Effects of the Iron Complexes of HDpT Analogues on DNA Plasmid DNA Integrity. It has been previously shown that some chelators prevent Fe-dependent hydroxyl-radical-mediated strand breaks in plasmid DNA, while others accelerate it.[10,40,57] Hence, we examined the effect of several **H**DpT ligands on Fe-mediated hydroxyl radical damage to plasmid DNA (Figure 6A,B).[50,57] We compared **H**DpT which does not have marked antiproliferative activity (IC_{50} = 5.2 μM; Table 3) to two chelators that showed highest redox activity in the ascorbate and benzoate hydroxylation assays, namely **H**Dp4mT and **H**Dp44mT, and possessed pronounced antiproliferative efficacy, i.e., IC_{50} = 0.18 μM and 0.01 μM, respectively (Table 3).

In all experiments, the following controls were included: untreated plasmid and plasmid treated with H_2O_2 that both run on gels as a major band of supercoiled (SC) DNA with a smaller proportion of plasmid in the open-circular (OC) form (Figure 6A; lanes 1 and 2). Plasmid treated with the restriction enzyme *Bam*H1 results in a single band of linearized DNA (Figure 6A; lane 3). In the ascorbate oxidation and benzoate hydroxylation assays, EDTA was redox-active, but this chelator was protective of SC and OC DNA at an IBE ratio of 3 (Figure 6A; lane 4). This result agreed with the well-characterized protective effects of EDTA against Fe-mediated DNA damage.[50,57] This can be explained by the repulsion of the anionic EDTA−Fe complex from the negatively charged polynucleotide molecule, preventing the targeting of the hydroxyl radicals to DNA. As shown before, in the presence of Fe^{II} and H_2O_2, DFO at an IBE ratio of 3 was also protective at preventing SC and OC DNA degradation (Figure 6A; lane 5). When plasmid was treated with Fe^{II} and H_2O_2 (Figure 6A; lane 6), SC and OC DNA was totally degraded due to Fe-induced hydroxyl-radical-mediated strand breaks. In contrast to DFO and EDTA, 3-AP (Figure 6A; lanes 16−18) did not prevent the ability of Fe^{II} to cause total degradation of plasmid DNA, as reported previously.[10]

The **H**DpT analogues differed in their ability to be protective of SC DNA in the presence of Fe^{II} and H_2O_2. **H**DpT demonstrated similar activity to 3-AP, with both chelators not preventing Fe^{II}-mediated degradation of DNA (Figure 6A; cf. lanes 7−9 to 16−18). Similarly, **H**Dp4mT did not prevent degradation of SC DNA at any IBE, but prevented degradation of OC DNA at an IBE of 3 only (Figure 6A; lane 12). DNA degradation in the presence of **H**Dp44mT was less marked than the other **H**DpT analogues, being protective of OC DNA at an IBE of 1 and preventing degradation of OC and SC DNA at an IBE of 3 (Figure 6A; lanes 13−15). Hence, while **H**Dp44mT showed very high antiproliferative activity, its ability to prevent plasmid DNA degradation was less marked than that observed with the **H**DpT analogue with lowest antiproliferative efficacy (Table 3). These results could potentially be explained by the different charge of the resulting Fe complexes that would affect their association with DNA and its subsequent degradation. The association of these **H**DpT ligands and their complexes with DNA was then assessed to determine this.

DNA Interactions of the HDpT Analogues and Their Fe Complexes. A decrease in UV−vis absorbance (hypochromicity) or an increase in UV−vis absorbance (hyperchromicity) upon addition of DNA to a compound in solution is indicative of an interaction between these molecules.[58−61] The ability of chelators and their Fe^{II} complexes to interact with DNA was determined by DNA-mediated hypochromicity and hyperchromicity of the UV−vis spectra.[58−61] The DNA-intercalating agent, DOX, was used as a relevant positive control for association with DNA.[50,62] DOX exhibited 25% and 36% hypochromicity as the Fe^{II} complex and free ligand, respectively (Figure 7). The decreased association with DNA observed by the Fe^{II} complex of DOX could be reflective of stereochemical constraints of the more bulky Fe complexes and/or the role of charge in DNA-binding activity.

Compared to DOX, the **H**DpT series showed lower association with DNA (Figure 7). The most active **H**DpT series chelator in terms of DNA association was **H**DpT that demonstrated 7% and 12% hypochromicity as the ligand and Fe^{II} complex, respectively (Figure 7). **H**Dp4mT and, particularly, **H**Dp44mT did not markedly interact with DNA as either the ligands or Fe^{II} complexes (Figure 7). These results agree with the plasmid DNA integrity assay. Indeed, **H**DpT did not protect plasmid DNA integrity, probably due to its ability to associate with DNA and target its redox activity, leading to DNA degradation (Figure 6A,B). In contrast, **H**Dp44mT and, to a lesser extent, **H**Dp4mT were somewhat protective of plasmid integrity at an IBE of 3. This is probably because the Fe complex does not markedly associate with DNA to target hydroxyl radical damage.

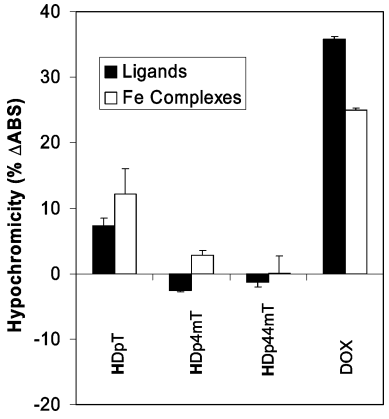

Figure 7. Ability of doxorubicin (DOX) and the di-2-pyridyl ketone thiosemicarbazone (**H**DpT) analogues to bind DNA. The ability of the chelators and their Fe^{II} complexes to bind DNA was determined through measurement of the DNA-mediated hypochromicity of ligand and Fe^{II} complex spectra. Data are expressed as the percentage decrease in peak absorbance intensity upon addition of DNA. Results are mean ± SEM (four experiments).

Implications of the Redox and DNA-Binding Activities of the HDpT Analogues. The combination of the ascorbate oxidation, benzoate hydroxylation, and plasmid DNA degradation assays, together with studies on DNA-binding and electrochemistry, provide information on the redox activity of the **H**DpT analogues. For one of the most active ligands in terms of antiproliferative activity, namely **H**Dp44mT (Table 3), its complex had an $Fe^{III/II}$ redox potential (+166 mV; Table 4) that would enable facile cycling between the Fe^{II} and Fe^{III} states. This compound was the most active in terms of ascorbate oxidation and benzoate hydroxylation (Figure 5A,B). However, **H**Dp44mT did not result in plasmid degradation (Figure 6A,B), since the complex did not associate with DNA to target its redox activity (Figure 7).

Despite **H**Dp4pT having high antiproliferative activity (Table 3), it did not demonstrate any ability to facilitate ascorbate oxidation or benzoate hydroxylation (Figure 5A,B). It is significant that the redox potential of this complex is the highest of the series (+225 mV; Table 4), and thus, the ferric oxidation state is much less accessible from a thermodynamic perspective. In other words, oxidation of the ferrous complex of **H**Dp4pT with H_2O_2 to initiate benzoate hydroxylation is sluggish. Similarly, regeneration of the ferric oxidation state (through aerobic oxidation) which is required for ascorbate oxidation is slow. This behavior mirrors that of the high potential PKIH−Fe^{II} complexes.[40] Hence, relatively small changes in ligand structure markedly alter the detection of redox activity by these latter two assays. Indeed, **H**Dp4pT was the only member of the six **H**DpT analogues that did not show any marked redox activity in either the ascorbate or benzoate hydroxylation assays (Figure 5A,B), and further studies on understanding its antiproliferative activity are warranted.

Conclusions

The current study demonstrates a number of important structure−activity relationships in the design of chelators for the treatment of cancer. In fact, the higher antiproliferative activity of the **H**DpT series of chelators[23] relative to the **H**PKIH class[22] can be ascribed, at least in part, to the electrochemical potentials of their Fe complexes which lead to ROS generation. In fact, the **H**DpT Fe complex redox potentials (+153 to +225 mV) are 300−400 mV lower than those of the PKIH−Fe^{II} complexes (ca. +500 mV)[40] and are accessible to cellular oxidants and reductants. However, this is not the only factor that is important. The most active **H**DpT ligands possess considerable lipophilicity and are neutral at physiological pH (Table 2 and Figure 3), allowing them to permeate cell membranes and bind cellular Fe pools more readily than less lipid-soluble chelators, e.g., DFO. Hence, the ability of these ligands to bind intracellular Fe and generate ROS is similar to the mechanism of action of the cytotoxic agent DOX and provides a "double punch". This is an important structure−activity relationship that should be encompassed into the design of future ligands for the treatment of cancer. Considering this, another important structural feature of antitumor Fe chelators deduced from examination of the **H**PKIH and **H**DpT ligands is the thioamide (NH−C═S) moiety. This group, in contrast to that of the amide group of the **H**PKIH hydrazone analogues, facilitates reversible $Fe^{III/II}$ redox reactions which are important for pronounced antiproliferative activity.

Experimental Section

Chemical Studies: Syntheses. Desferrioxamine (DFO) and doxorubicin (DOX) were obtained from Novartis (Basel, Switzerland) and Pharmacia (Sydney, Australia), respectively. The precursors thiosemicarbazide, 4-methyl-3-thiosemicarbazide, 4-ethyl-3-thiosemicarbazide, 4,4-dimethyl-3-thiosemicarbazide, 4-phenyl-3-thiosemicarbazide, 4-allyl-3-thiosemicarbazide, and di-2-pyridyl ketone were obtained from Sigma-Aldrich, and all solvents used were of analytical purity.

Physical Methods. NMR spectra were measured at 500 MHz on a Bruker instrument. IR spectra were measured on a Perkin-Elmer 1600 series spectrophotometer using an ATR (attenuated total reflectance) assembly. Electrospray ionization mass spectrometry (ESI-MS) was performed on a Kratos MS25 instrument with methanolic solutions of each sample. UV−vis spectra were measured on an Analytik Jena Specord 210 spectrophotometer. Cyclic voltammetry was performed with a BAS100B/W potentiostat. A glassy carbon working electrode, an aqueous Ag/AgCl reference, and Pt wire auxiliary electrode were used. All complexes were at ca. 1 mM concentration in MeCN:H_2O 70:30 v/v. The supporting electrolyte was Et_4NClO_4 (0.1 M), and the solutions were purged with nitrogen prior to measurements.

Elemental analysis (C, H, N) of the ligands and complexes was performed, and the results, available as Supporting Information, were within ±0.4% of the theoretical values, unless otherwise stated.

Free Ligands. A. Di-2-pyridyl Ketone 4-Methyl-3-thiosemicarbazone (HDp4mT). Di-2-pyridyl ketone (1.934 g, 10 mmol) was dissolved in EtOH (15 mL). A solution of 4-methyl-3-thiosemicarbazide (1.194 g, 10 mmol) in water (15 mL) was added followed by glacial acetic acid (5 drops) and the mixture refluxed for 2 h. The mixture was cooled to ca. 5 °C, and the yellow precipitate was collected by vacuum filtration and washed with EtOH then diethyl ether. This afforded **H**Dp4mT (67%) as yellow crystals: ^{1}H NMR ($CDCl_3$) δ 8.79 (dq, 1H), 8.62 (dq, 1H), 7.81 (td, 1H), 7.71−7.77 (m, 2H), 7.48 (dt, 1H), 7.32−7.36 (m, 3H), 3.24 (d, 3H); IR (ATR) 3266s, 3052m, 1587w, 1534s, 1454m, 1431m, 1311s, 1251w, 1223s, 1152m, 1111s, 1038s, 961w, 825s, 800s, 735s, 675s, 648s cm^{-1}. Anal. Calcd ($C_{13}H_{13}N_5S$): C, 57.55; H, 4.83; N, 25.81. Found: C, 57.1; H, 4.8; N, 25.5.

All other thiosemicarbazones were prepared in the same way using the appropriate thiosemicarbazides.

B. Di-2-pyridyl Ketone 4-Ethyl-3-thiosemicarbazone (HDp4eT) (from 4-Ethyl-3-thiosemicarbazide). This gave **H**Dp4eT (56%) as yellow crystals: ^{1}H NMR ($CDCl_3$) δ 8.79 (dq, 1H), 8.62 (dq, 1H), 7.81 (td, 1H), 7.71−7.77 (m, 2H), 7.47 (dt, 1H), 7.33−7.36 (m, 3H), 3.76 (m, 2H), 1.28 (t, 3H); IR (ATR) 3190m, 1582m, 1536s, 1453vs, 1309s, 1276w, 1251w, 1216s, 1195s, 1155m, 1106s, 1064m, 997m, 936w, 889vw, 816m, 796ws, 741s, 674m, 651s, 613s, 600s cm^{-1}. Anal. ($C_{14}H_{15}N_5S$) C, H, N.

C. Di-2-pyridyl Ketone 4-Phenyl-3-thiosemicarbazone (HDp4pT) (from 4-Phenyl-3-thiosemicarbazide). HDp4pT (72%) was col-

lected as yellow crystals: ^{1}H NMR ($CDCl_3$) δ 9.54 (s, 1H), 8.84 (d, 1H), 8.68 (dq, 1H), 7.86 (td, 1H), 7.79−7.83 (m, 2H), 7.70 (d, 2H), 7.37−7.42 (m, 4H), 7.23 (tt, 1H); IR (ATR) 3449m, 3197m, 1590s, 1529vs, 1480w, 1459w, 1435m, 1319m, 1252w, 1215vw, 1173vs, 1110s, 995w, 928w, 803m, 762m, 694m, 650w cm^{-1}. Anal. ($C_{18}H_{15}N_5S$) C, H, N.

D. Di-2-pyridyl Ketone 4-Allyl-3-thiosemicarbazone (HDp4aT) (from 4-Allyl-3-thiosemicarbazide). This afforded **H**Dp4aT (68%) as yellow crystals: ^{1}H NMR ($CDCl_3$) δ 8.79 (d, 1H), 8.62 (d, 1H), 7.70−7.84 (m, 4H), 7.49 (d, 1H), 7.34 (q, 1H), 5.95 (m, 1H), 5.2 (dd, 1H), 4.39 (t, 2H); IR (ATR) 3450w, 3150s, 1643w, 1584m, 1528vs, 1466s, 1420m, 1307s, 1252w, 1189s, 1114s, 996m, 920s, 830m, 797s, 722m, 682w, 656m, 613s cm^{-1}. Anal. ($C_{15}H_{15}N_5S$) C, H, N.

E. Di-2-pyridyl Ketone 4,4-Dimethyl-3-thiosemicarbazone (HDp44mT) (from 4,4-Dimethyl-3-thiosemicarbazide). HDp44mT (87%) was collected as yellow crystals: ^{1}H NMR ($CDCl_3$) δ 8.67 (dd, 1H), 8.55 (dd, 1H), 8.09 (d, 1H), 7.80 (m, 2H), 7.67 (dd, 1H), 7.35 (dt, 1H), 7.28 (dt, 1H), 3.45 (s, 6H); IR (ATR) 3449vs, 3054w, 1654w, 1511m, 1438w, 1373m, 1311vs, 1236s, 1190w, 1127m, 1003s, 972w, 907m 806s, 731s, 651s cm^{-1}. Anal. Calcd ($C_{14}H_{15}N_5S$): C, 58.93; H, 5.30; N, 24.54. Found: C, 58.3; H, 5.4; N, 23.9.

F. Di-2-pyridyl Ketone Thiosemicarbazone (HDpT) (from Thiosemicarbazide). H DpT (83%) was afforded as yellow crystals: ^{1}H NMR ($CDCl_3$) δ 8.79 (dq, 1H), 8.62 (dq, 1H), 7.74−7.84 (m, 3H), 7.51 (dt, 1H), 7.46 (s br, 1H), 7.34−7.39 (m, 2H), 6.38 (s, 1H); IR (ATR) 3303s, 1624s, 1587m, 1488s, 1460s, 1329m, 1251s, 1109s, 1067s, 996m, 845s, 800s, 682w cm^{-1}. Anal. ($C_{12}H_{11}N_5S$) C, H, N.

Iron Complexes. A. Fe^{III}L Complexes. The complexes were prepared by the following general method. The appropriate thiosemicarbazone (3.6 mmol) was dissolved in 15 mL of EtOH (15 mL), and Et_3N (0.37 g, 3.6 mmol) was added. To this solution was added $Fe(ClO_4)_3\cdot 6H_2O$ (0.849 g, 1.8 mmol), and the mixture was gently refluxed for 30 min. Upon cooling, the dark brown product was filtered off and washed with EtOH followed by ether.

1. [Fe(Dp4mT)$_2$]ClO$_4$·$^1/_2$H$_2$O. The complex (52%) was collected as a brown powder: IR (ATR) 3400s, 1554s, 1500m, 1447s, 1395s, 1347m, 1304m, 1274w, 1160m, 1086vs, 995w, 968w,788m, 745m, 655w, 621s cm^{-1}; Electronic spectrum (MeOH): λ_{max} 475 nm (ϵ 6 950 M^{-1} cm^{-1}), 379 (ϵ 19 240); LRMS (ESI) (MeOH): *m*/*z* (relative intensity), 596 (100%) ([M − ClO$_4$]$^+$, ([$C_{26}H_{24}N_{10}S_2Fe\cdot ClO_4$ − ClO$_4$]$^+$). Anal. ($C_{26}H_{25}ClFeN_{10}O_{4.5}S_2$) C, H, N.

2. [Fe(Dp4eT)$_2$]ClO$_4$·3H$_2$O. The complex (32%) was obtained as a brown solid: IR (ATR) 2982w, 1586w, 1545m, 1497w, 1421s, 1336m, 1297w, 1273w, 1207w, 1155w, 1074vs, 929w, 790s, 745s, 682w, 653w, 619s cm^{-1}; Electronic spectrum (MeOH): λ_{max} 463 nm (ϵ 5 170 M^{-1} cm^{-1}), 380 (ϵ 13 780); LRMS (ESI) (MeOH): *m*/*z* (relative intensity), 624 (100%) ([M − ClO$_4$]$^+$, ([$C_{28}H_{28}N_{10}S_2Fe\cdot ClO_4$ − ClO$_4$]$^+$). Anal. Calcd ($C_{28}H_{34}ClFeN_{10}O_7S_2$): C, 43.22; H, 4.40; N, 18.00. Found: C, 44.0; H, 4.1; N, 17.9.

3. [Fe(Dp44mT)$_2$]ClO$_4$·1$^1/_2$H$_2$O. The complex (60%) was collected as a brown powder: IR (ATR) 3417s, 1552s, 1504m, 1455m, 1395vs, 1317vs, 1252vs, 1085vs, 911m, 787w, 751w, 622m cm^{-1}; Electronic spectrum (MeOH): λ_{max} 486 nm (ϵ 10 340 M^{-1} cm^{-1}), 395 (ϵ 32 600); LRMS (ESI) (MeOH): *m*/*z* (relative intensity), 624 (100%) ([M − ClO$_4$]$^+$, ([$C_{28}H_{28}N_{10}S_2Fe^{III}$]$^+$). Anal. ($C_{28}H_{31}ClFeN_{10}O_{4.5}S_2$) C, H, N.

4. [Fe(Dp4pT)$_2$]ClO$_4$·2$^1/_2$H$_2$O. This afforded the complex (51%) as a brown solid: IR (ATR) 3047w, 1584m, 1493m, 1406s, 1344m, 1313m, 1181w, 1118m, 1094s, 1017w, 781w, 743vs, 690s, 616m cm^{-1}; Electronic spectrum (MeOH): λ_{max} 469 nm (ϵ 5 410 M^{-1} cm^{-1}), 368 (ϵ 10 870); LRMS (ESI) (MeOH): *m*/*z* (relative intensity), 720 (100%) ([M − ClO$_4$]$^+$, ([$C_{36}H_{28}N_{10}S_2Fe^{III}$]$^+$). Anal. Calcd ($C_{36}H_{33}ClN_{10}FeO_{6.5}S_2$): C, 49.98; H, 3.84; N, 15.97. Found: C, 49.2; H, 4.0; N, 16.0.

5. [Fe(Dp4aT)$_2$]ClO$_4$·4H$_2$O. The complex (26%) was collected as a brown solid: IR (ATR) 3400s, 1586m, 1545w, 1500m, 1413vs, 1317s, 1119vs, 994w, 788w, 746m, 687w, 621m cm^{-1}; Electronic spectrum (MeOH): λ_{max} 462 nm (ϵ 4 320 M^{-1} cm^{-1}), 381 (ϵ 21 700); LRMS (ESI) (MeOH): *m*/*z* (relative intensity), 648 (100%) ([M − ClO$_4$]$^+$, ([$C_{30}H_{28}N_{10}S_2Fe\cdot ClO_4$ − ClO$_4$]$^+$). Anal. Calcd ($C_{30}H_{36}ClFeN_{10}O_8S_2$): C, 43.94; H, 4.42; N, 17.08. Found: C, 43.90; H, 3.91; N, 16.33.

6. [Fe(DpT)$_2$]ClO$_4$. The complex (34%) was obtained as a brown powder: IR (ATR) 3296m, 1589m, 1492w, 1418s, 1327s, 1216w, 1147s, 953w, 785w, 747w, 684w, 622w cm^{-1}; Electronic spectrum (MeOH): λ_{max} 460 nm (ϵ 6 770 M^{-1} cm^{-1}), 365 (ϵ 12 340); LRMS (ESI) (MeOH): *m*/*z* (relative intensity), 568 (100%) ([M − ClO$_4$]$^+$, ([$C_{24}H_{20}N_{10}S_2Fe.ClO_4$ − ClO$_4$]$^+$). Anal. Calcd ($C_{24}H_{20}ClFeN_{10}O_4S_2$): C, 43.16; H, 3.02; N, 20.97. Found: C, 44.3; H, 3.9; N, 21.0.

B. Fe^{II}L Complexes. The Fe(II) complexes were prepared by the following general method. The thiosemicarbazone (3.2 mmol) was dissolved in EtOH (15 mL), and 0.37 g of Et_3N was added to the solution under nitrogen gas. Then 0.652 g of $Fe(ClO_4)_2\cdot 6H_2O$ was added to the basic ligand solution, and the mixture was gently refluxed for 30 min under nitrogen. Upon cooling the green product was filtered off by vacuum filtration and washed with EtOH followed by ether.

1. [Fe(Dp4mT)$_2$]·H$_2$O. The Fe(Dp4mT)$_2$ complex (80%) was obtained as a green powder: IR (ATR) 3256s, 1586s, 1536s, 1490w, 1422s, 1389s, 1341s, 1293s, 1153s, 1096w, 1032w, 784m, 743s, 642w cm^{-1}; Electronic spectrum (MeOH): λ_{max} 643 nm (ϵ 8 040 M^{-1} cm^{-1}), 380 (ϵ 22 850); LRMS (ESI) (MeOH): *m*/*z* (relative intensity), 596 (100%) ([M − e]$^+$, ([$C_{26}H_{24}N_{10}S_2Fe^{III}$]$^+$). Anal. Calcd ($C_{26}H_{26}FeN_{10}OS_2$): C, 50.82; H, 4.26; N, 22.79. Found: C, 51.4; H, 4.0; N, 23.1.

2. [Fe(Dp4eT)$_2$]·1.5H$_2$O. The Fe(Dp4eT)$_2$ complex (77%) was collected as a green solid: IR (ATR) 3277w, 2969w, 1586m, 1561w, 1523m, 1433w, 1408vs, 1334s, 1290s, 1206w, 1148m, 1119w, 1083w, 1049w, 1017m, 994w, 967w, 782m, 744s, 648w, 619w cm^{-1}; Electronic spectrum (MeOH): λ_{max} 644 nm (ϵ 7 450 M^{-1} cm^{-1}), 379 (ϵ 28 830); LRMS (ESI) (MeOH): *m*/*z* (relative intensity), 624 (100%) ([M − e]$^+$, ([$C_{28}H_{28}N_{10}S_2Fe^{III}$]$^+$). Anal. ($C_{28}H_{31}N_{10}FeO_{1.5}S_2$) C, H, N.

3. [Fe(Dp44mT)$_2$]·H$_2$O. The Fe(Dp44mT)$_2$ complex (72%) was obtained as a green powder: IR (ATR) 3436m, 1582s, 1517w, 1385s, 1320s, 1237s, 1148s, 914s, 784m, 743s, 633m, 550m cm^{-1}; Electronic spectrum (MeOH): λ_{max} 646 nm (ϵ 10 840 M^{-1} cm^{-1}), 390 (ϵ 30 040); LRMS (ESI) (MeOH): *m*/*z* (relative intensity), 624 (100%) ([M − e]$^+$, ([$C_{28}H_{28}N_{10}S_2Fe^{III}$]$^+$). Anal. Calcd ($C_{28}H_{30}FeN_{10}OS_2$): C, 52.34; H, 4.71; N, 21.80. Found: C, 52.9; H, 4.5; N, 22.0.

4. [Fe(Dp4pT)$_2$]·1$^1/_2$H$_2$O. The Fe(Dp4pT)$_2$ complex (58%) was collected as a green powder: IR (ATR) 3052w, 1586m, 1494m, 1474m, 1408vs, 1344m, 1316m, 1251m, 1184w, 1121m, 1098w, 1019w, 995w, 974vw, 781w, 744s, 692s, 616w cm^{-1}; Electronic spectrum (MeOH): λ_{max} 630 nm (ϵ 7 200 M^{-1} cm^{-1}), 393 (ϵ 24 540); LRMS (ESI) (MeOH): *m*/*z* (relative intensity), 720 (100%) ([M − e]$^+$, ([$C_{36}H_{28}N_{10}S_2Fe^{III}$]$^+$). Anal. ($C_{36}H_{31}FeN_{10}O_{1.5}S_2$) C, H, N.

5. [Fe(Dp4aT)$_2$]·3.5H$_2$O. The Fe(Dp4aT)$_2$ complex (32%) was obtained as a green powder: IR (ATR) 3399s, 1585m, 1498m, 1411s, 1273s, 1090s, 787m, 744s, 620s cm^{-1}; Electronic spectrum (MeOH): λ_{max} 626 nm (ϵ 3 850 M^{-1} cm^{-1}), 379 (ϵ 26 300); LRMS (ESI) (MeOH): *m*/*z* (relative intensity), 648 (100%) ([M − e]$^+$, ([$C_{30}H_{28}N_{10}S_2Fe^{III}$]$^+$). Anal. Calcd ($C_{30}H_{35}FeN_{10}O_{3.5}S_2$): C, 45.12; H, 4.29; N, 17.54. Found: C, 45.8; H, 3.8; N, 17.6.

6. [Fe(DpT)$_2$]·3H$_2$O. The Fe(DpT)$_2$ complex (79%) was obtained as a green powder: IR (ATR) 3292m, 1620w, 1587m, 1494w, 1460w, 1412s, 1323s, 1132s, 783m, 747s, 550w cm^{-1}; Electronic spectrum (MeOH): λ_{max} 644 nm (ϵ 5 270 M^{-1} cm^{-1}), 365 (ϵ 14 860); LRMS (ESI) (MeOH): *m*/*z* (relative intensity), 568 (100%) ([M − e]$^+$, [$C_{24}H_{20}N_{10}S_2Fe^{III}$]$^+$). Anal. Calcd ($C_{24}H_{26}N_{10}FeO_3S_2$): C, 46.31; H, 4.21; N, 22.50. Found: C, 47.0; H, 4.0; N, 22.8.

Potentiometric Titrations. These were performed under a nitrogen atmosphere in a water-jacketed chamber maintained at 298 K, using a Metrohm 796 Titroprocessor equipped with a 10 mL 700 Dosino automatic buret and a Metrohm AG CH-9101 combined glass electrode, as described.[39] The electrode was calibrated by a strong acid−strong base titration prior to each experiment. Typical

pK_w values of ca. 13.7 were obtained consistently. In all ligand titrations, the titrant was 0.1 M Et_4NOH, standardized with HCl, and the reaction vessel was blanketed with nitrogen to exclude CO_2. Data obtained were refined by a nonlinear least-squares refinement method using the program TITFIT[63] to determine pK_a values. In each case, a minimum of three titrations were performed in the range $2 < pH < 12$ using 0.5−1 mM solutions of free ligands acidified with dilute $HClO_4$. The supporting electrolyte was 0.1 M Et_4NClO_4.

Crystallography. Cell constants at 293 K were determined by a least-squares fit to the setting parameters of 25 independent reflections measured on an Enraf-Nonius CAD4 four-circle diffractometer employing graphite-monochromated Mo Kα radiation (0.71073 Å) and operating in the ω-2θ scan mode within the range $2 < 2\theta < 50$ Å. Data reduction and empirical absorption corrections (ψ-scans) were performed with the WINGX suite of programs.[64] Structures were solved by direct methods with SHELXS and refined by full-matrix least-squares analysis with SHELXL-97.[65] All non-H atoms were refined with anisotropic thermal parameters. Aryl and amino H-atoms were included at estimated positions using a riding model. Water and amide H-atoms (if any) were first located from difference maps and then restrained at these positions in a manner similar to that employed for the remaining H-atoms. Molecular structure diagrams were produced with ORTEP3.[66] The data in CIF format has been deposited at the Cambridge Crystallographic Data Centre with deposition numbers 608888 and 608889.

Biological Studies: Cell Culture. The human SK-N-MC neuroepithelioma cell line was obtained from the American Type Culture Collection (ATCC; Rockville, MD). The cells were grown as described.[19,20]

Effect of the Chelators on Cellular Proliferation. This was examined using the MTT (3-(4,5-dimethylthiazol-2-yl)-2,5-diphenyl tetrazolium) assay as described.[19,20] MTT color formation was directly proportional to the number of viable cells measured by Trypan blue staining.[19]

Ascorbate Oxidation Assay. An established protocol was used to measure ascorbate oxidation.[1,10,40,50,67] Briefly, ascorbic acid (100 μM) was prepared immediately prior to an experiment and incubated in the presence of Fe(III) (10 μM; added as $FeCl_3$), a 50-fold molar excess of citrate (500 μM), and the chelator (1−60 μM). Absorbance at 265 nm was measured after 10 and 40 min at room temperature and the decrease of intensity between these time points calculated.[50,67]

Benzoate Hydroxylation. This assay employs benzoate as a hydroxyl radical scavenger to generate fluorescent salicylate as a product (308 nm excitation and 410 nm emission) using a standard protocol.[10,40,50,67] Briefly, benzoic acid (1 mM) was incubated for 1 h at room temperature in 10 mM disodium hydrogen phosphate (pH 7.4) with 5 mM hydrogen peroxide, the Fe chelator (3−180 μM), and ferrous sulfate (30 μM). All solutions were prepared immediately prior to use, and the Fe(II) was added to water that had been extensively purged with nitrogen. The addition of Fe was used to start the reaction, and the solution was kept in the dark prior to measuring the fluorescence using a Perkin-Elmer L550B spectrofluorometer. In these experiments, salicylate was used as a standard and to determine quenching by the chelators.[50,67]

Measurement of DNA Integrity Using the Plasmid pGEM-7Zf(+) in the Presence of Fe and the Chelator. The measurement of plasmid integrity was performed using standard techniques as described previously.[10,40,50] Briefly, the plasmid pGEM-7Zf(+) (Promega Inc.) was purified using the Qiagen plasmid purification kit (Qiagen Inc., USA). Reagents were added to sterile Eppendorf tubes in the following order: purified sterile water, chelator (1, 10, and 30 μM), $FeSO_4$ (10 μM), H_2O_2 (1 mM), and plasmid DNA (10 μg/mL). Samples were incubated at room temperature for 30 min with these solutions, and 25 μL aliquots were immediately loaded with 5 μL of loading dye onto a 1% agarose gel containing ethidium bromide. As controls, plasmid linearized with *Bam*H1, plasmid alone, plasmid incubated with H_2O_2, and plasmid incubated with Fe and H_2O_2 were used. Electrophoresis was performed for 1 h at 90 V in Tris-borate buffer containing 0.5 M EDTA. After migration, the DNA was visualized using a UV-transilluminator and photographed.

DNA-Binding Assay. The ability of ligands or Fe complexes to bind DNA was measured via DNA-mediated hypochromicity and hyperchromicity of the ligand or Fe complex UV−vis absorbance spectra.[58−61] An appropriate absorbance peak was chosen from spectrophotometric wavelength scans of each chelator and its Fe complex. Concentrations of test compounds were then adjusted so that peak absorbance intensities were less than 1. Herring sperm DNA (Sigma) was added to ligand, Fe complex, or reference solutions to a final nucleotide concentration 3.6 times that of the test compound.[58,59,68] Following 10 min incubation at room temperature, DNA-dependent hypochromic (decrease in UV−vis absorbance) or hyperchromic (increase in UV−vis absorbance) changes in test compound peak absorbance were calculated. It was not possible to measure interactions of this kind for EDTA or DFO, as these ligands have inadequate peaks in their UV−vis absorbance spectra. The well-characterized DNA-intercalation agent, namely DOX, was used as a positive control.[50,62,69,70]

In all experiments examining the redox properties of chelators, the data was expressed as iron-binding equivalents (IBE). This was due to the different coordination modes of the ligands to Fe, i.e., DFO and EDTA are hexadentate and form 1:1 ligand:Fe complexes, while the HDpT analogues are tridentate resulting in 2:1 complexes. Hence, for a direct comparison of the hexadentate and tridentate ligands, it was necessary to add twice as much tridentate as hexadentate chelator. In the present study, a range of ligand:Fe IBE ratios were used, namely 0.1, 1, or 3. An IBE of 0.1 represents an excess of Fe to chelator, i.e., 1 hexadentate chelator or 2 tridentate chelators in the presence of 10 Fe atoms. An IBE of 1 is equivalent to the complete filling of the coordination sphere, i.e. Fe:EDTA 1:1 or Fe:DpT 1:2, while an IBE of 3 represents an excess of chelator to Fe and is equal to either 3 hexadentate or 6 tridentate ligands in the presence of 1 Fe atom.

Statistical Analysis. Experimental data were compared using Student's *t*-test. Results were expressed as mean or mean ± SD (number of experiments) and considered statistically significant when $p < 0.05$.

Acknowledgment. D.R.R. and P.V.B. thank the Australian Research Council of Australia for research grant funding. D.R.R. acknowledges the National Health and Medical Research Council of Australia for grant and fellowship support. D.K. is the grateful recipient of an Australian Post-graduate Award from the University of Sydney (DP0450001).

Supporting Information Available: Crystallographic information and elemental analysis data in tabular format. This material is available free of charge via the Internet at http://pubs.acs.org.

References

(1) Bergeron, R. J.; Wiegand, J.; McManis, J. S.; Bussenius, J.; Smith, R. E. et al. Methoxylation of desazadesferrithiocin analogues: enhanced iron clearing efficiency. *J. Med. Chem.* **2003**, *46*, 1470−1477.

(2) Bergeron, R. J.; Huang, G.; Weimar, W. R.; Smith, R. E.; Wiegand, J. et al. Desferrithiocin analogue based hexacoordinate iron(III) chelators. *J. Med. Chem.* **2003**, *46*, 16−24.

(3) Richardson, D. R. The therapeutic potential of iron chelators. *Expert Opin. Invest. Drugs* **1999**, *8*, 2141−2158.

(4) Richardson, D. R. Molecular mechanisms of iron uptake by cells and the use of iron chelators for the treatment of cancer. *Curr. Med. Chem.* **2005**, *12*, 2711−2729.

(5) Buss, J. L.; Torti, F. M.; Torti, S. V. The role of iron chelation in cancer therapy. *Curr. Med. Chem.* **2003**, 10, 1021−1034.

(6) Regino, C. A.; Torti, S. V.; Ma, R.; Yap, G. P.; Kreisel, K. A. et al. N-Picolyl derivatives of Kemp's triamine as potential antitumor agents: a preliminary investigation. *J. Med. Chem.* **2005**, *48*, 7993−7999.

(7) Torti, S. V.; Ma, R.; Venditto, V. J.; Torti, F. M.; Planalp, R. P. et al. Preliminary evaluation of the cytotoxicity of a series of tris-2-aminoethylamine (Tren) based hexadentate heterocyclic donor agents. *Bioorg. Med. Chem.* **2005**, *13*, 5961−5967.

(8) Larrick, J. W.; Cresswell, P. Modulation of cell surface iron transferrin receptors by cellular density and state of activation. *J. Supramol. Struct.* **1979**, *11*, 579−586.
(9) Cooper, C. E.; Lynagh, G. R.; Hoyes, K. P.; Hider, R. C.; Cammack, R. et al. The relationship of intracellular iron chelation to the inhibition and regeneration of human ribonucleotide reductase. *J. Biol. Chem.* **1996**, *271*, 20291−20299.
(10) Chaston, T. B.; Lovejoy, D. B.; Watts, R. N.; Richardson, D. R. Examination of the antiproliferative activity of iron chelators: multiple cellular targets and the different mechanism of action of triapine compared with desferrioxamine and the potent pyridoxal isonicotinoyl hydrazone analogue 311. *Clin. Cancer Res.* **2003**, *9*, 402−414.
(11) Nyholm, S.; Mann, G. J.; Johansson, A. G.; Bergeron, R. J.; Graslund, A. et al. Role of ribonucleotide reductase in inhibition of mammalian cell growth by potent iron chelators. *J. Biol. Chem.* **1993**, *268*, 26200−26205.
(12) Blatt, J.; Stitely, S. Antineuroblastoma activity of desferoxamine in human cell lines. *Cancer Res.* **1987**, *47*, 1749−1750.
(13) Wang, F.; Elliott, R. L.; Head, J. F. Inhibitory effect of deferoxamine mesylate and low iron diet on the 13762NF rat mammary adenocarcinoma. *Anticancer Res.* **1999**, *19*, 445−450.
(14) Donfrancesco, A.; Deb, G.; Dominici, C.; Angioni, A.; Caniglia, M. et al. Deferoxamine, cyclophosphamide, etoposide, carboplatin, and thiotepa (D-CECaT): a new cytoreductive chelation-chemotherapy regimen in patients with advanced neuroblastoma. *Am. J. Clin. Oncol.* **1992**, *15*, 319−322.
(15) Estrov, Z.; Tawa, A.; Wang, X. H.; Dube, I. D.; Sulh, H. et al. In vitro and in vivo effects of deferoxamine in neonatal acute leukemia. *Blood* **1987**, *69*, 757−761.
(16) Donfrancesco, A.; Deb, G.; Dominici, C.; Pileggi, D.; Castello, M. A. et al. Effects of a single course of deferoxamine in neuroblastoma patients. *Cancer Res.* **1990**, *50*, 4929−4930.
(17) Richardson, D. R. Iron chelators as therapeutic agents for the treatment of cancer. *Crit. Rev. Oncol. Hematol.* **2002**, *42*, 267−281.
(18) Kalinowski, D. S.; Richardson, D. R. The evolution of iron chelators for the treatment of iron overload disease and cancer. *Pharmacol. Rev.* **2005**, *57*, 547−583.
(19) Richardson, D. R.; Tran, E. H.; Ponka, P. The potential of iron chelators of the pyridoxal isonicotinoyl hydrazone class as effective antiproliferative agents. *Blood* **1995**, *86*, 4295−4306.
(20) Richardson, D. R.; Milnes, K. The potential of iron chelators of the pyridoxal isonicotinoyl hydrazone class as effective antiproliferative agents II: the mechanism of action of ligands derived from salicylaldehyde benzoyl hydrazone and 2-hydroxy-1-naphthylaldehyde benzoyl hydrazone. *Blood* **1997**, *89*, 3025−3038.
(21) Lovejoy, D. B.; Richardson, D. R. Novel "hybrid" iron chelators derived from aroylhydrazones and thiosemicarbazones demonstrate selective antiproliferative activity against tumor cells. *Blood* **2002**, 100, 666−676.
(22) Becker, E. M.; Lovejoy, D. B.; Greer, J. M.; Watts, R.; Richardson, D. R. Identification of the di-pyridyl ketone isonicotinoyl hydrazone (PKIH) analogues as potent iron chelators and anti-tumour agents. *Br. J. Pharmacol.* **2003**, *138*, 819−830.
(23) Yuan, J.; Lovejoy, D. B.; Richardson, D. R. Novel di-2-pyridyl-derived iron chelators with marked and selective antitumor activity: in vitro and in vivo assessment. *Blood* **2004**, *104*, 1450−1458.
(24) Richardson, D. R., Wis Vitolo, L. M., Hefter, G. T., May, P. M., Clare, B. W., Webb, J., Wilairat, P. Iron chelators of the pyridoxal isonicotinoyl hydrazone class Part I. Ionization characteristics of the ligands and their relevance to biological properties. *Inorg. Chim. Acta* **1990**, *170*, 165−170.
(25) Bergeron, R. J.; Bharti, N.; Wiegand, J.; McManis, J. S.; Yao, H. et al. Polyamine-vectored iron chelators: the role of charge. *J. Med. Chem.* **2005**, *48*, 4120−4137.
(26) Philip, V.; Suni, V.; Kurup, M. R. P. Di-2-pyridyl ketone 4-methyl-4-phenylthiosemicarbazone. *Acta Crystallogr., Sect. C* **2004**, *C60*, o856−o858.
(27) Suni, V.; Kurup, M. R. P.; Nethaji, M. Structural and spectral perspectives of a novel thiosemicarbazone synthesized from di-2-pyridyl ketone and 4-phenyl-3-thiosemicarbazide. *Spectrochim. Acta, Part A* **2006**, *63A*, 174−181.
(28) Swearingen, J. K.; Kaminsky, W.; West, D. X. Structural and spectral studies of di-2-pyridyl ketone 3-piperidyl- and 3-hexamethyleneiminylthiosemicarbazone and their cobalt(II), nickel(II) and copper(II) complexes. *Transition Met. Chem. (Dordrecht)* **2002**, *27*, 724−731.
(29) Duan, C.-Y.; Wu, B.-M.; Mak, T. C. W. Synthesis and structural characterization of the new quadridentate N3S-compound di-2-pyridyl ketone thiosemicarbazone and its binuclear copper(II) complexes. *J. Chem. Soc., Dalton Trans.* **1996**, 3485−3490.
(30) Usman, A.; Razak, I. A.; Chantrapromma, S.; Fun, H. K.; Philip, V. et al. Di-2-pyridyl ketone N4,N4-(butane-1,4-diyl)thiosemicarbazone. *Acta Crystallogr., Sect. C* **2002**, *C58*, o652−o654.
(31) Swearingen, J. K.; West, D. X. Structural and spectral studies of di-2-pyridyl ketone N(4)-methyl- and N(4)-dimethylthiosemicarbazone and their metal complexes. *Transition Met. Chem. (Dordrecht)* **2001**, *26*, 252−260.
(32) Bergeron, R. J.; Wiegand, J.; McManis, J. S.; Vinson, J. R.; Yao, H. et al. (S)-4,5-dihydro-2-(2-hydroxy-4-hydroxyphenyl)-4-methyl-4-thiazolecarboxylic acid polyethers: a solution to nephrotoxicity. *J. Med. Chem.* **2006**, *49*, 2772−2783.
(33) Baker, E.; Richardson, D.; Gross, S.; Ponka, P. Evaluation of the iron chelation potential of hydrazones of pyridoxal, salicylaldehyde and 2-hydroxy-1-naphthylaldehyde using the hepatocyte in culture. *Hepatology* **1992**, *15*, 492−501.
(34) Ponka, P.; Richardson, D. R.; Edward, J. T.; Chubb, F. L. Iron chelators of the pyridoxal isonicotinoyl hydrazone class. Relationship of the lipophilicity of the apochelator to its ability to mobilise iron from reticulocytes in vitro. *Can. J. Physiol. Pharmacol.* **1994**, *72*, 659−666.
(35) Edward, J. T.; Ponka, P.; Richardson, D. R. Partition-coefficients of the iron(III) complexes of pyridoxal isonicotinoyl hydrazone and its analogues and the correlation to iron chelation efficacy. *Biometals* **1995**, *8*, 209−217.
(36) Rai, B. L.; Dekhordi, L. S.; Khodr, H.; Jin, Y.; Liu, Z. D. et al. Synthesis, physicochemical properties, and evaluation of N-substituted-2-alkyl-3-hydroxy-4(1H)-pyridinones. *J. Med. Chem*. **1998**, *41*, 3347−3359.
(37) Thomas, F.; Baret, P.; Imbert, D.; Pierre, J. L.; Serratrice, G. Partition coefficients (free ligands and their iron(III) complexes) and lipophilic behavior of new abiotic chelators. Correlation to biological activity. *Bioorg. Med. Chem. Lett.* **1999**, *9*, 3035−3040.
(38) Edward, J. T.; Chubb, F. L.; Sangster, J. Iron chelators of the pyridoxal isonicotinoyl hydrazone class. Relationship of the lipophilicity of the apochelator to its ability to mobilize iron from reticulocytes in vitro: reappraisal of reported partition coefficients. *Can. J. Physiol. Pharmacol.* **1997**, *75*, 1362−1368.
(39) Bernhardt, P. V.; Chin, P.; Sharpe, P. C.; Wang, J. Y.; Richardson, D. R. Novel diaroylhydrazine ligands as iron chelators: coordination chemistry and biological activity. *J. Biol. Inorg. Chem.* **2005**, 10, 761−777.
(40) Bernhardt, P. V.; Caldwell, L. M.; Chaston, T. B.; Chin, P.; Richardson, D. R. Cytotoxic iron chelators: characterization of the structure, solution chemistry and redox activity of ligands and iron complexes of the di-2-pyridyl ketone isonicotinoyl hydrazone (HP-KIH) analogues. *J. Biol. Inorg. Chem.* **2003**, *8*, 866−880.
(41) Chaston, T. B.; Watts, R. N.; Yuan, J.; Richardson, D. R. Potent antitumor activity of novel iron chelators derived from di-2-pyridylketone isonicotinoyl hydrazone involves Fenton-derived free radical generation. *Clin. Cancer Res.* **2004**, *10*, 7365−7374.
(42) Xu, X.; Persson, H. L.; Richardson, D. R. Molecular pharmacology of the interaction of anthracyclines with iron. *Mol. Pharmacol.* **2005**, *68*, 261−271.
(43) Richardson, D. R.; Bernhardt, P. V. Crystal and molecular structure of 2-hydroxy-1-naphthaldehyde isonicotinoyl hydrazone (NIH) and its iron(III) complex: an iron chelator with anti-tumour activity. *J. Biol. Inorg. Chem.* **1999**, *4*, 266−273.
(44) Johnson, D. K.; Pippard, M. J.; Murphy, T. B.; Rose, N. J. An in vivo evaluation of iron-chelating drugs derived from pyridoxal and its analogs. *J. Pharmacol. Exp. Ther.* **1982**, *221*, 399−403.
(45) Richardson, D. R. Cytotoxic analogs of the iron(III) chelator pyridoxal isonicotinoyl hydrazone: effects of complexation with copper(II), gallium(III), and iron (III) on their antiproliferative activities. *Antimicrob. Agents Chemother.* **1997**, *41*, 2061−2063.
(46) Johnson, D. K., Murphy, T. B., Rose, N. J., Goodwin W. H., Pickart, L. Cytotoxic chelators and chelates 1. Inhibition of DNA synthesis in cultured rodent and human cells by aroylhydrazones and by a copper(II) complex of salicylaldehyde benzoyl hydrazone. *Inorg. Chim. Acta* **1982**, *67*, 159−165.
(47) Feun, L.; Modiano, M.; Lee, K.; Mao, J.; Marini, A. et al. Phase I and pharmacokinetic study of 3-aminopyridine-2-carboxaldehyde thiosemicarbazone (3-AP) using a single intravenous dose schedule. *Cancer Chemother. Pharmacol.* **2002**, *50*, 223−229.
(48) Bernhardt, P. V.; Mattsson, J.; Richardson, D. R. Complexes of cytotoxic chelators from the dipyridyl ketone isonicotinoyl hydrazone (HPKIH) analogues. *Inorg. Chem.* **2006**, *45*, 752−760.
(49) Chaston, T. B.; Richardson, D. R. Iron chelators for the treatment of iron overload disease: relationship between structure, redox activity, and toxicity. *Am. J. Hematol.* **2003**, *73*, 200−210.
(50) Chaston, T. B.; Richardson, D. R. Interactions of the pyridine-2-carboxaldehyde isonicotinoyl hydrazone class of chelators with iron and DNA: implications for toxicity in the treatment of iron overload disease. *J. Biol. Inorg. Chem.* **2003**, *8*, 427−438.
(51) Verma, P. S.; Saxena, R. C.; Jayaraman, A. Cyclic voltammetric studies of certain industrially potential iron chelate catalysts. *Fresenius' J. Anal. Chem.* **1997**, *357*, 56−60.

(52) Spasojevic, I.; Armstrong, S. K.; Brickman, T. J.; Crumbliss, A. L. Electrochemical behavior of the Fe(III) complexes of the cyclic hydroxamate siderophores alcaligin and desferrioxamine E. *Inorg. Chem.* **1999**, *38*, 449−454.
(53) Giles, F. J.; Fracasso, P. M.; Kantarjian, H. M.; Cortes, J. E.; Brown, R. A. et al. Phase I and pharmacodynamic study of Triapine, a novel ribonucleotide reductase inhibitor, in patients with advanced leukemia. *Leuk. Res.* **2003**, *27*, 1077−1083.
(54) Murren, J.; Modiano, M.; Clairmont, C.; Lambert, P.; Savaraj, N. et al. Phase I and pharmacokinetic study of triapine, a potent ribonucleotide reductase inhibitor, administered daily for five days in patients with advanced solid tumors. *Clin. Cancer Res.* **2003**, *9*, 4092−4100.
(55) Wadler, S.; Makower, D.; Clairmont, C.; Lambert, P.; Fehn, K. et al. Phase I and pharmacokinetic study of the ribonucleotide reductase inhibitor, 3-aminopyridine-2-carboxaldehyde thiosemicarbazone, administered by 96-hour intravenous continuous infusion. *J. Clin. Oncol.* **2004**, *22*, 1553−1563.
(56) Yee, K. W.; Cortes, J.; Ferrajoli, A.; Garcia-Manero, G.; Verstovsek, S. et al. Triapine and cytarabine is an active combination in patients with acute leukemia or myelodysplastic syndrome. *Leuk. Res.* **2006**.
(57) Hermes-Lima, M.; Nagy, E.; Ponka, P.; Schulman, H. M. The iron chelator pyridoxal isonicotinoyl hydrazone (PIH) protects plasmid pUC-18 DNA against *OH-mediated strand breaks. *Free Radical Biol. Med.* **1998**, *25*, 875−880.
(58) Jin, L.; Yang, P. Synthesis and DNA binding studies of cobalt (III) mixed-polypyridyl complex. *J. Inorg. Biochem.* **1997**, *68*, 79−83.
(59) Mudasir; Yoshioka, N.; Inoue, H. DNA binding of iron(II) mixed-ligand complexes containing 1,10-phenanthroline and 4,7-diphenyl-1,10-phenanthroline. *J. Inorg. Biochem.* **1999**, *77*, 239−247.
(60) Trommel, J. S.; Marzilli, L. G. Synthesis and DNA binding of novel water-soluble cationic methylcobalt porphyrins. *Inorg. Chem.* **2001**, *40*, 4374−4383.
(61) Zhang, Q. L.; Liu, J. G.; Chao, H.; Xue, G. Q.; Ji, L. N. DNA-binding and photocleavage studies of cobalt(III) polypyridyl complexes. *J. Inorg. Biochem.* **2001**, *83*, 49−55.
(62) Cummings, J.; Bartoszek, A.; Smyth, J. F. Determination of covalent binding to intact DNA, RNA, and oligonucleotides by intercalating anticancer drugs using high-performance liquid chromatography. Studies with doxorubicin and NADPH cytochrome P-450 reductase. *Anal. Biochem.* **1991**, *194*, 146−155.
(63) Zuberbuehler, A. D.; Kaden, T. A. TITFIT, a comprehensive program for numerical treatment of potentiometric data by using analytical derivatives and automatically optimized subroutines with the Newton-Gauss-Marquardt algorithm. *Talanta* **1982**, *29*, 201−206.
(64) Farrugia, L. J. WINGX − an integrated system of Windows programs for the solution, refinement and analysis of single-crystal X-ray diffraction data. *J. Appl. Crystallogr.* **1999**, *32*, 837−838.
(65) Sheldrick, G. M. *SHELX97. Programs for Crystal Structure Analysis*, Release 97-2 ed.; University of Göttingen: Göttingen, Germany.
(66) Farrugia, L. J. ORTEP-3 for windows − a version of ORTEP-III with a graphical user interface (GUI). *J. Appl. Crystallogr.* **1997**, *30*, 565.
(67) Dean, R. T.; Nicholson, P. The action of nine chelators on iron-dependent radical damage. *Free Radical Res.* **1994**, *20*, 83−101.
(68) Cusumano, M.; Giannetto, A. The interaction of mixed-ligand square-planar complexes with calf thymus DNA. *J. Inorg. Biochem.* **1997**, *65*, 137−144.
(69) Kellogg, G. E.; Scarsdale, J. N.; Fornari, F. A., Jr. Identification and hydropathic characterization of structural features affecting sequence specificity for doxorubicin intercalation into DNA double-stranded polynucleotides. *Nucleic Acids Res.* **1998**, *26*, 4721−4732.
(70) Kostoryz, E. L.; Yourtee, D. M. Oxidative mutagenesis of doxorubicin-Fe(III) complex. *Mutat. Res.* **2001**, *490*, 131−139.

JM0606342